



Advanced Representative Rail Temperature Measurement Point Considering Rail Deformation by Meteorological Conditions and Rail Orientation

Cheoljeong Park¹ · Jongwon Yoon¹ · Sunguk Hong¹ · Chan Park¹ · Yeondo Jeong¹ · Jungmin Kim¹ · Byeongjun Lee¹ · Haran Lee¹ · Chiwon Song¹ · Seong J. Cho¹ 

Received: 7 July 2022 / Revised: 4 November 2022 / Accepted: 8 November 2022 / Published online: 14 December 2022

© The Author(s), under exclusive licence to Korean Society for Precision Engineering 2022

Abstract

Rail temperature is the main effector of train operation. High rail temperature induces rail deformation and because of limited space for rail deformation, rails are under compressive pressure. When rail deformation is exceeded, rail buckling occurs, and this causes rail derailment. Although such a rail derailment is infrequent, the casualties of human lives and properties are catastrophic. To prevent this, the rail industry has been monitoring rail temperature. However, existing representative rail temperature measurement points (RMPs) are selected without considering thermal deformation, and there is no sufficient information for selecting RMPs. In this study, we suggest a novel advanced RMP (ARMP) considering rail installation orientation and meteorological conditions. We designed a measurement system for rail temperature and obtained 1-year data of rail temperature at multiple internal, external rail points and the surrounding environments. We validated our measured data with field data similar to the climate in which the measurement system was installed. The maximum error and Mean Absolute Error (MAE) were 3.3 °C and 0.97 °C respectively. We calculated average deformation points (ADPs) and analyzed them with respect to the energy that the rail receives from the meteorological conditions, which are represented by the cumulative amount of solar irradiance and installation orientation. Based on the tendency of ADPs, we suggested a simple equation of ARMP with only one variable, month. ARMP showed high accuracy in measuring rail temperature at two installation orientations than previous RMPs (R-square: 0.9255, 0.8577 and MAE: 0.21 °C, 0.33 °C). We expect that this study would contribute to efficient train operation for the precise measurement of rail temperature.

Keywords Rail temperature · Rail deformation · Buckling · Temperature distribution · Temperature monitoring

1 Introduction

High climate temperatures caused by abnormal climate are detrimental to rail conditions [1–4]. High climate temperature increases rail temperature, which causes rail deformation. Rail deformation places a rail under compressive pressure, and rail buckling occurs when the pressure is exceeded. Rail buckling can stop or delay a train operation system; in the worst case, it can trigger a train derailment, resulting in catastrophic loss [5, 6]. The train industry

usually places a free space between a rail for deformation to prevent buckling. Recently, the train industry has been using continuous welded rails (CWRs), which weld the free space between rails for high-speed trains. CWRs can provide comfortable and high-speed travel, but lack of clearance makes CWRs to be compressively stressed and causes rail buckling [7–9]. Because of the trade-off relationship between the risk of buckling and CWR use, the train industry focuses on monitoring rail temperature to prevent buckling and provide high-speed train services [10]. When a high rail temperature is detected, actions are taken to lower it, e.g., spraying water and applying thermal paint to the rail. In addition, when these actions are difficult to implement, the train speed is limited to prevent derailment. In Korea, the high-speed train, Korean Train Express (KTX), runs under the speed limit regulations that limit its speed with respect to rail temperature [11]. The

✉ Seong J. Cho
scho@cnu.ac.kr

¹ Department of Mechanical Engineering, Chungnam National University, 99 Daehak-ro, Yuseong-gu, Daejeon 34134, Republic of Korea

train should run below 230 km/h at 55–60 °C rail temperature, below 70 km/h at 60–64 °C rail temperature, and stop running above 64 °C rail temperature. In the United Kingdom, train speed is also determined by the stress-free rail temperature. Therefore, the accurate measurement of rail temperature is crucial for safe [12] and efficient train operation.

However, it is difficult to directly measure rail temperature over an entire network. To alleviate the difficulty, Hunt and Esveld developed a simple model to predict rail temperature from air temperature to replace direct measurement [6, 7]. Chapman et al. [11] also proposed a novel model to predict rail temperature from not only air temperature but also weather data such as solar irradiance. In addition, a more complex but more accurate model was proposed by Wu et al. [13]. These models are based on the strong relationship between rail temperature and air temperature. However, they can only be used in limited environments and are difficult to be used in the real field because of their low accuracy.

Moreover, despite the relevance of accurate measurement, an rail temperature measurement point is selected and used in an rail temperature monitoring system without considering rail deformation according to the surrounding climate, although rail temperature monitoring is to prevent rail deformation from exceeding the allowable level. To alleviate this limitation, Hong et al. [14] suggested a representative rail temperature measurement point (RMP) for the KS-50 N rail considering meteorological conditions and rail deformation, which could represent rail temperature over the entire network. They designed an rail temperature measurement system and measured rail temperature inside and outside of the KS-50 N rail at 500 mm and calculated average deformation according to the surrounding climate. They also analyzed the average deformation point (ADP) at which the temperature represents rail deformation by the surrounding climate.

However, the above studies have limitations. First, the adequacy of the measured data was not evaluated. Data evaluation should be performed before analysis to evaluate the adequacy of a measurement system. Second, the rail installation orientation was not considered. Chapman, Hong and Urakawa's studies respectively showed that there is a temperature difference with respect to rail installation orientation because of the sun's daily path and difference in solar incidence area [11, 14–17]. Whittingham's study [18] also showed that there are different patterns of rail temperature depending on the rail installation orientation. These differences affect rail deformation and may affect suggesting an appropriate RMP. Third, their analyses did not include analysis over time. They analyzed ADP by overall tendency and weather (sunny, cloudy, and rainy days) but did not consider time, although rail temperature mainly varies with time. To efficiently operate a train system and prevent rail buckling and derailment, it is essential to select an RMP considering

rail deformation according to the surrounding climate and its orientation.

In this study, we suggested an Advanced RMP (ARMP) for the UIC-60 rail, which is commonly used as a high-speed train track, considering the meteorological conditions and rail installation orientation. Particularly, we designed and installed a measurement system that simulates the rail's real environment of operation at Chungnam National University (CNU), Yuseong-gu, Daejeon, Republic of Korea, and measured rail temperature and surrounding climate data. We compared the measured rail data with data measured at the Daejeon train station, Yuseong-gu, Daejeon, Republic of Korea, to evaluate our data's adequacy. We analyzed the rail temperature data and showed the difference with respect to installation orientation. We performed deformation analysis using the finite element method (FEM) and calculated ADP. We analyzed ADP with respect to time and month and showed its tendency, which is significantly influence rail temperature measurement. Based on the ADP tendency, we suggested the ARMP. The ARMP has a simple second-order equation with one variable, month. It showed high accuracy and reliability, with 0.9255 and 0.8587 in R-square at 0° and 90° installation orientations, respectively. Also, we suggested Fixed Representative rail-temperature Measurement Point (FRMP), which may user preferred, and it also showed high reliability (MAE, ARMP showed 0.21 and 0.33 at each direction). We expect that the suggested ARMP and FRMP of UIC-60 rail will be used in the rail maintenance field, especially monitoring system of rail temperature including predicting rail t and support efficient rail operation.

2 Methods

This study was conducted in three major steps: (1) the measurement and verification of data, (2) rail deformation analysis and ADP calculation, and (3) ARMP suggestion (Fig. 1). We designed measurement system for obtaining dataset of rail temperature and its surrounding environment. After measurement, dataset was verified with real-field dataset at Okcheon station, Republic of Korea. With verified and filtered dataset, FEM analysis and ADP calculation was conducted with ANSYS and Python. We analyzed ADP by the energy rail gets and its installation orientation and suggest ARMP. The details are described below.

2.1 Measurement System

Measuring rail temperature of a rail in operation is difficult because of safety issues. We designed a measurement system similar to the actual railroad at CNU, as shown Fig. 2a, b. The designed system was installed where the shadow effect was minimized to imitate the open environment of

a rail system. We used four 500-mm UIC-60 rails, which are mainly used as a high-speed track in Korea, and installed these rails in a two-way direction: two rails in the north–south direction (0° orientation) and two rails in the east–west direction (90° orientation). Each rail was installed on a ballast and concrete sleeper. We used resistance temperature detectors (RTDs) and K-type thermocouples to measure rail temperature; each rail had multiple measurement points (Fig. 2c). On rails 2, 3, and 4 (Fig. 2d), 16 measurement points were designed; we installed RTDs at eight interior points and eight surface points. On rail 1, 29 measurement points were designed; we installed RTDs at 10 interior points and K-type thermocouples at 19 surface points. Details of the measurement points are shown in Additional file 1: Figure S1. Particularly, we slightly ground a rail surface, attached an RTD and K-type thermocouple at the surface using heat-transferable epoxy, and taped to fix the RTD's position. For interior measurement points, we drilled holes on rails and inserted RTDs and K-type thermocouples. Then, we filled the holes with heat-transferable epoxy, which helped the sensors measure internal rail temperature accurately. We employed a weather station (Vantage Pro2, Davis) to measure weather data simultaneously. Specifically, we measured air temperature, solar irradiance, wind speed, humidity, and rainfall at the weather station. At the weather station, RTDs and thermocouples were connected to a data acquisition system, and the system measured rail and climate data in a 10-min sampling time.

2.2 Data Verification and Rail Temperature Analysis

Data verification that the designed measurement system measures field rail temperature is needed before analyzing rail temperature and longitudinal deformation. We verified our measured data by comparison with rail temperature data measured at Okcheon, Republic of Korea. The Okcheon data were measured in an open environment in which the shadow effect is minimized and is similar to our measurement environment at CNU. The Okcheon data have been used for operating train systems. Therefore, we set the Okcheon data as true values of rail temperature and verified our data using the mean absolute error (MAE) index. Because the measurement sites differ, we selected sunny day data and compared rail temperature at the same point.

After verifying our data and the adequacy of the designed system's representativity, we analyzed the rail temperature difference between rails installed at different orientations (north–south and east–west directions). We compared rails 1–4 at the same measurement point. We selected the comparing measurement point at the rail center (90 mm from the bottom) because measurement points located at the surface can be easily affected by the sun and surrounding climate

and can cause an inappropriate comparison without considering appropriate control variables.

2.3 Calculation of Average Deformation Point (ADP)

One year measurement with a 10-min sampling time could yield enormous raw data. Using all data for FEM analysis was time-consuming and difficult to observe changes in deformation. Therefore, we set filtering criteria to filter useful data and perform efficient analysis.

First, we removed data with unexpected errors, e.g., measurement system, sensor replacement, sensor calibration, and data acquisition errors. For missing values measured incorrectly in less than 20 min (less than two steps of sampling time), we interpolated them using an average interpolation method.

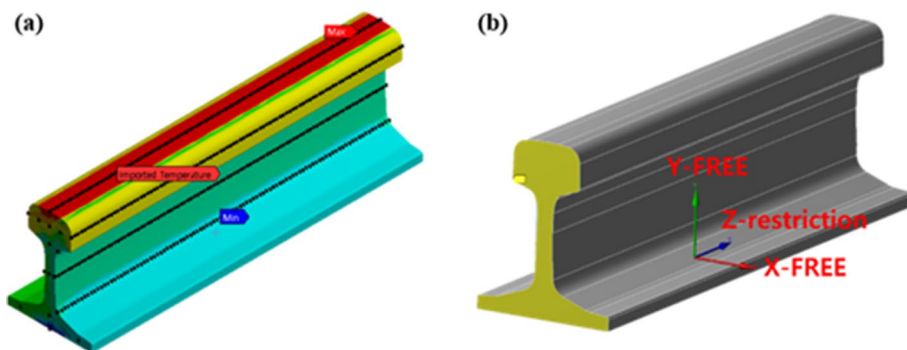
Second, we used daytime data measured from 08:00 to 06:00 p.m. We focused on rail deformation, particularly buckling, so we did not select nighttime data for deformation analysis because there were only minute rail temperature variations. However, in summer when sunset was later than 06:00 p.m., we also used data at 07:00 p.m. Meanwhile, in winter, when sunset was earlier than 06:00 p.m. (very close to 06:00 p.m.), we exceptionally used data at 06:00 p.m., although there was no measured solar irradiance at that time.

Third, to observe significant deformation, we used O'clock data. Several 10-min sampling data points could make the analysis complicated and could not show significant deformation differences within 10 min because of a small temperature variation. To avoid these situations and observe significant changes in temperature and deformation, we set this term.

Fourth, we did not use temperature data changed below 0.3°C . Small temperature changes in 60 min could show minute deformation variations.

With the above criteria, we could improve ADP analysis accuracy while increasing the efficiency of the total analysis. We performed FEM analysis for thermal deformation with the FEM software, ANSYS. We designed a model using Steady-State and Static Structural tools in ANSYS. First, using the Steady-State tool, we performed temperature interpolation to determine the rail temperature distribution with the interior and surface rail temperature data measured at UIC-60 rails. Second, we set the model's boundary conditions and mesh (Additional file 1: Figure S2). We solely fixed the degree of freedom in the rails' longitudinal Z-axis direction during the ANSYS implementation. Meanwhile, the X- and Y-axis deformation were left free (Fig. 3). The model's mesh was generated uniformly in every analysis. Using the Static Structural tool, we performed thermal deformation analysis to determine longitudinal deformation on the rail model, which was critical to rail buckling. Third, we calculated the rails' ADPs. ADP is the point that can

Fig. 3 Setting of deformation analysis on ANSYS (a) inserted measured data (dot points) and interpolated temperature on rail (b) boundary condition



represent a rail’s average deformation and the temperature that caused the deformation. We used Python code to calculate the rails’ ADPs and displayed the positional data on a UIC-60 rail image (Fig. 4). In this image, we can obtain the average deformation line. For the last step, to select an ADP from the average deformation line, we only used the ADP at the rail’s centerline ($X=0$) because of the rail’s symmetrical shape. Consequently, we could select a single ADP per analysis using only Y coordinate variations.

2.4 Calculation of Advanced Representative Rail-Temperature Measurement Point (ARMP)

To suggest an ARMP, we performed a statistical analysis on the calculated ADP data. We selected solar irradiance (a major heat source on rail), installation orientation, and time as our analysis parameters. Solar irradiance causes rail deformation. Installation orientation changes solar incidence area, causing differences in rail temperature, which induces different rail deformations. The intensity of solar irradiance varies with time; thus, time is also a major parameter influencing rail temperature and rail deformation. We analyzed the tendency of the calculated ADP data with respect to

these parameters and suggested an ARMP; the details are shown below.

First, we analyzed ADP data with respect to the energy the rail receives to determine the behavior of ADP with respect to cumulative energy and installation orientation. We employed the cumulative amount of solar irradiance (CASI), which can represent the energy the rail receives with respect to time, also employed by Hong et al. [13]. We separated the calculated ADP data with respect to CASI levels. We set CASI levels to three levels on an average of seasonal and timely CASI. We set a low level, below 3500 W/m^2 of CASI (an average of 1 year’s morning before 10 a.m.); a middle level, between 3500 and $25,000 \text{ W/m}^2$ (an average of 1 year’s daytime); and a high level, above $25,000 \text{ W/m}^2$ (usually in a scorching day). With the three CASI levels, we analyzed each level and found appropriate average points.

Second, we analyzed the calculated ADP data by month. The former step showed the relationship between ADP and CASI; thus, in this step, we analyzed the monthly behavior of ADP. CASI varies daily, but to observe a clear difference, we set the period for each month. We analyzed the calculated ADP monthly and realized the tendency of ADP.

Finally, we suggested an ARMP and a fixed representative rail temperature measurement point (FRMP) from the

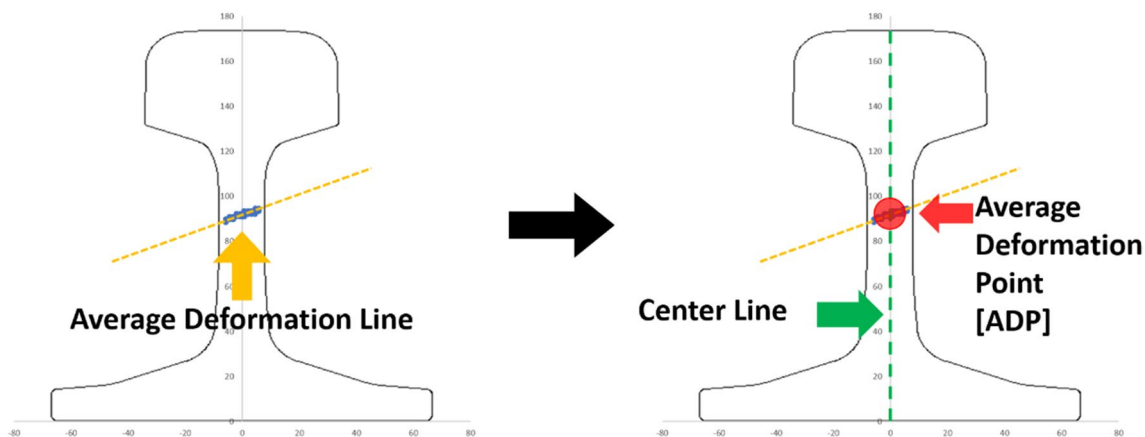


Fig. 4 Process of calculating average deformation line and ADP on UIC-60 rail

analysis. We evaluated ARMP and FRMP by R-square and MAE to assess their precision. In evaluating temperature difference, we used measured rail temperature and simply interpolated rail temperature where it was not measured.

3 Results and Discussion

3.1 Rail Temperature Analysis by Orientation of Rail

We measured rail temperature at multiple points of the rail and climate data for one year (from July 20, 2018, to July 20, 2019) with a 10-min sampling time. We removed about 21 days of data based on the abovementioned standard, and most of the data were found in February 2019. As such, the February dataset is smaller than those of other months. We collected about 5,200,000 rail temperature and climate data points.

We verified our data measured at CNU using the Okcheon data. We selected the data of 13 sunny days at both sites to verify our dataset. On verification, the MAE of air temperature was 0.83 °C, and the maximum error was 1.5 °C, indicating that the measurement environments of both sites are similar. As shown in Additional file 1: Figure S2, rail temperature showed similar patterns at both sites. The maximum error and MAE were 3.3 °C and 0.97 °C, respectively. These errors were due to different measurement conditions—installation orientations. However, a small MAE showed that our measurement system is representative of rail temperature in an actual field.

Previous studies have shown that rail temperature differs with respect to its installation orientation [11–14, 18]. We compared rail temperature on the same point at different rail orientations to confirm this. As shown in Fig. 5, the north–south rail (0° orientation) and east–west (90° orientation) showed differences in rail temperature. In summer, from June to July, rail temperature difference with respect to

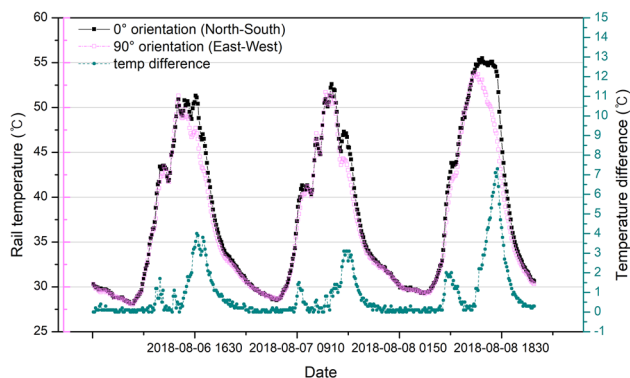


Fig. 5 Temperature differences between different orientations (August 6–10, 2018)

installation orientation was up to 7.3 °C; it was up to 9.4 °C in autumn (from September to November) and spring (from March to May) and up to 9 °C in winter (from December to February). These differences occur owing to differences in the rail solar incidence area with respect to installation orientation. Because of these differences, rail has different rail temperature distributions at different installation orientations, thereby causing different RDs at the same time.

3.2 Average Deformation Point (ADP) Analysis

We performed an additional filtering process with filtering criteria before analyzing RD considering the meteorological conditions to determine clear differences. We could obtain 15,476 datasets of rail temperature and climate data. After the filtering process, we performed the FEM analysis with ANSYS. We performed deformation analysis more than 30,000 times and collected about 16,000 RD data points in a 60-min interval. We calculated ADPs and analyzed them with respect to energy and time to suggest an ARMP.

ADP is based on longitudinal RD, which is mainly affected by the surrounding climate and environment. We analyzed the behavior of ADP in terms of the energy the rail receives and selected CASI—a factor that can represent how much energy the rail receives—as an ADP parameter. Figure 6 shows the entire ADP data in terms of CASI levels, whereas Additional file 1: Figures S3 and S4 show the data separated monthly. In the two considered orientations, ADP converged around 90 mm from the rail bottom. Particularly, at 0° and 90° orientations, the mean of ADP showed 90.07 mm (standard deviation: 20.30 mm) and 85.90 mm (standard deviation: 15.25 mm), respectively. This difference is due to the difference in the rail’s solar incidence area, which causes an imbalance in the rail temperature distribution and local RD. Therefore, ADP is positioned more widely where local RD more frequently occurs.

Also shown in Fig. 7, ADP showed different distributions with respect to CASI levels. We separated ADPs by the suggested CASI levels and analyzed them. At the low CASI level, when the rail received small energy, ADP showed a large deviation, indicating that rail temperature increased locally and deformation occurred locally because of the small energy. For both installation orientations, the low CASI level showed the highest deviation. At the mid-CASI level, ADPs showed the minimum deviation and converged at 90 mm. ADPs varied more at the high CASI level than at the mid-CASI level. The results indicate that at the low and high CASI levels, there is an imbalance of rail temperature distribution and rail deformation. This imbalance does not cause unexpected accidents at the low CASI level, whereas it can cause rail buckling and train derailment at the high CASI level.

Fig. 6 Relationship between CASI and position of ADP

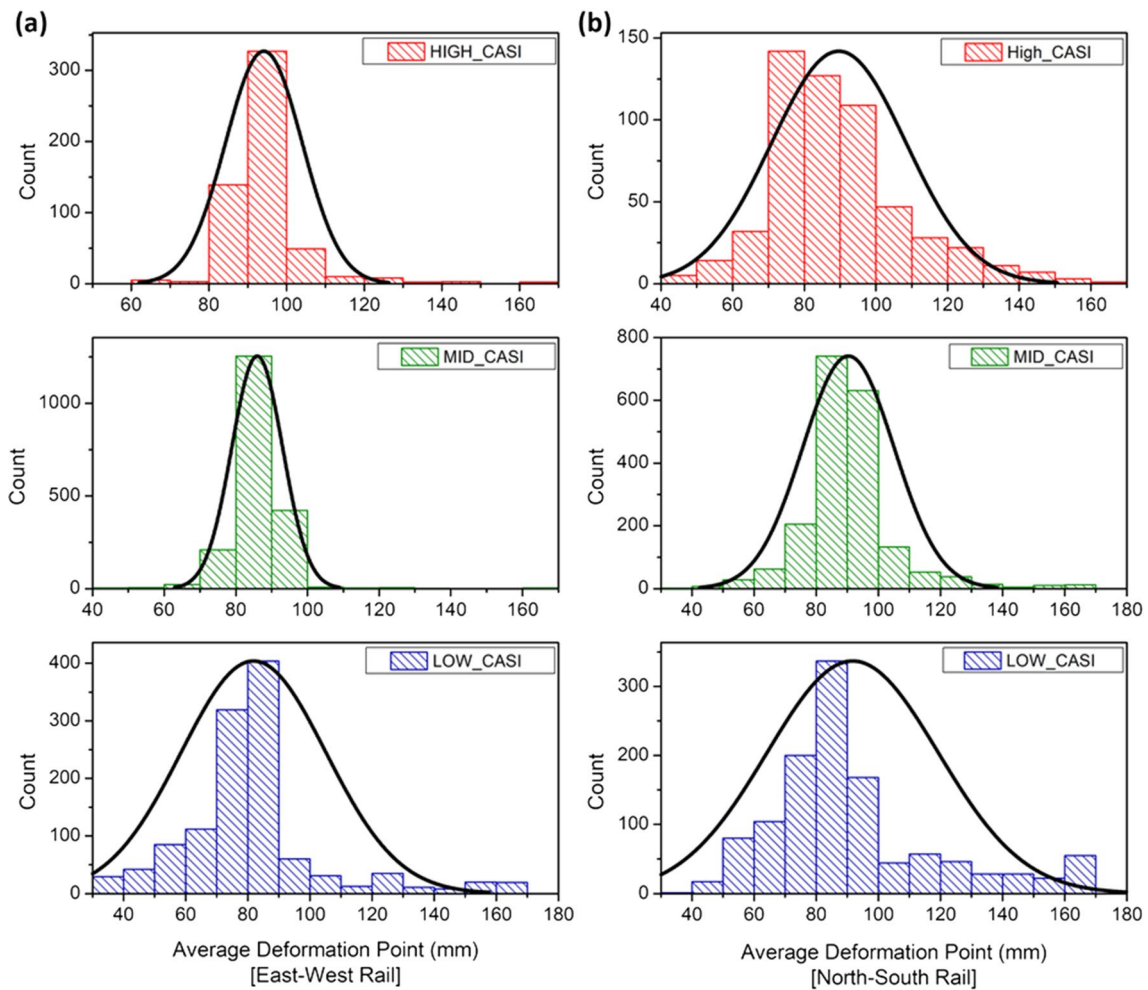
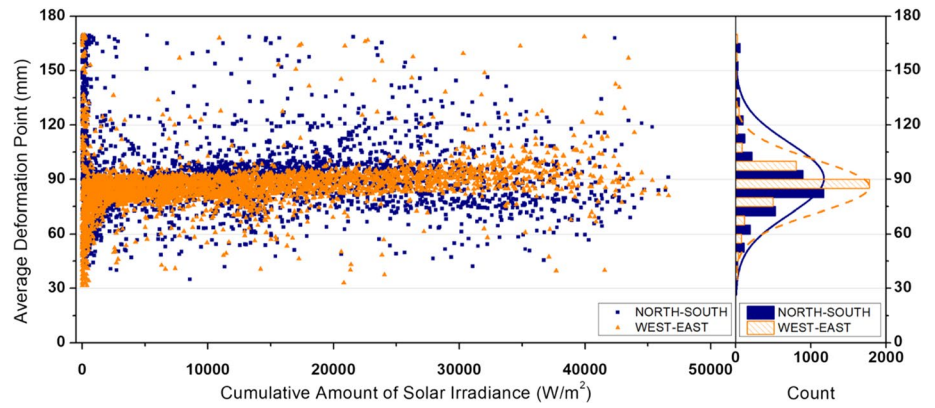


Fig. 7 Histogram and normal distribution of ADP in terms of Cumulative Amount of Solar irradiance (CASI) level level (a) ADP distribution of East–West rail (90° orientation) (b) ADP distribution of North–South Rail (0° orientation)

We also analyzed ADP with respect to month because CASI varies with time. Additional file 1: Table S1 summarizes the mean and standard deviation of ADP with respect to month and installation orientation. The results at the two installation orientations showed that ADP was

around 90 mm but also showed a difference with respect to its installation orientation. In addition, the results showed minimum and maximum means of ADP in winter and summer, respectively. In winter, the sun is positioned near the perihelion, which means the nearest to the Earth, and CASI

is the maximum at that time. However, ADP is minimized because our measurement system is located in the northern hemisphere. In summer, the sun is positioned around the apex, which means the farthest from the Earth. CASI is minimized throughout the year, but ADP is maximized for the same reason as above. These showed that ADP is governed by the sun’s position and installation orientation.

We also showed the tendency of ADP with respect to month (Fig. 8). As mentioned above, ADP varied with respect to energy, which is represented by CASI, and time. This showed that the mean of ADP differs with respect to CASI; particularly, it has a linear relationship with CASI. In other words, the relationship between ADP and CASI can be simplified by the relationship between ADP and month, which has a clear difference from CASI. Therefore, we used this simplified relationship to suggest an ARMP.

3.3 Advanced Representative Rail-Temperature Measurement Point (ARMP) Analysis

We constructed monthly mean of ADP regression equations that could calculate the monthly mean of ADP. These equations are illustrated in Table 1. In Table 1, y represents the measurement point, and x represents the month. The actual values of the mean of ADP and the MAE of the mean of ADP derived by the equations show a difference of 0.21 and 0.33 mm at 0° and 90° orientations, respectively. Rail temperature at these points, is able to represent temperature of the UIC-60 rail considering its deformation and installation orientation. As shown in Fig. 9, we suggested this equation as Advanced Representative rail-temperature Measurement Point (ARMP). We also calculated mean of these points by its orientation respectively and suggested these points as Fixed rail-temperature Measurement Point (FRMP) which was simply following a previous study of rail-temperature representative point of KS-50n rail [14]. In comparison

ARMP showed 22.1% better performance than FRMP in the respect of MAE. Both ARMP and FRMP showed high reliability and accuracy and by the purpose or user’s preference both suggested points are able to contribute precise rail temperature measurement. For example, in the train industry, 1 °C of rail temperature can change rail operation speed and evaluate rail condition, furthermore, decide when to implement actions to lower rail temperature by rail-engineers. For an efficient train system, precisely measuring rail temperature at an appropriate point is required.

4 Conclusion

In this study, we analyzed longitudinal rail deformation and calculated ADP considering rail installation orientation. With the calculated ADP data, we analyzed the relationship between ADP and CASI and determined the tendency of

Table 1 Equation of ARMP and performance of ARMP and FRMP

	Equation	R ²	Temperature difference	
			MAE (°C)	Max error (°C)
0° orientation	$y = -0.475x^2 + 6.0639x + 71.817$	0.9255	0.21	0.42
90° orientation	$y = -0.2819x^2 + 3.3815x + 81.493$	0.8587	0.33	0.41
FRMP	$y = 90$	–	0.55	0.73

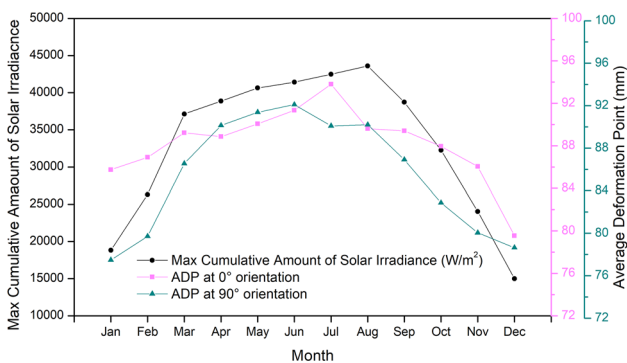


Fig. 8 Tendency of ADP with respect to month and installation orientation

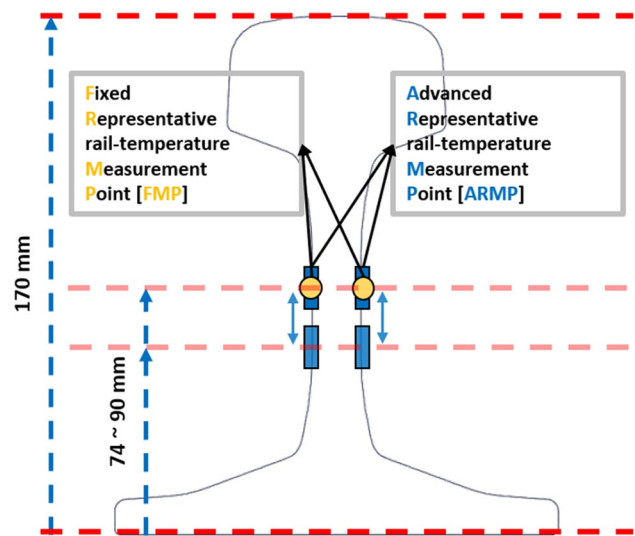


Fig. 9 Schematic of FRMP and ARMP

ADP by month considering installation orientation, which is significantly influence rail temperature measurement. Consequently, we suggested ARMP and FRMP for the UIC-60 rails. These points are more sensitive to rail deformation than conventional measurement points because they are suggested by considering rail deformation and rail installation orientation. ARMP and FRMP showed high reliability and accuracy (mean absolute error = 0.21 and 0.33 and maximum error = 0.42 and 0.41 for 0° and 90° installed orientations, respectively). We expect that this study will contribute to the rail industry, especially monitoring rail temperature and precisely measuring rail temperature, to prevent buckling accidents and serve efficient train services. In future studies, we will consider more variation of installation orientation to analyze its effects on ADP more precisely.

Supplementary Information The online version contains supplementary material available at <https://doi.org/10.1007/s12541-022-00747-7>.

Acknowledgements This work was supported by the National Research Foundation of Korea (NRF) grant funded by the Korea government (No. 2021R1I1A3055744 and No. 2021R1A4A1032762).

References

1. Stipanovic Oslakovic, I., Hartmann, A., & Dewulf, G. (2013). Risk assessment of climate change impacts on railway infrastructure. In *Proceedings of engineering project organization conference, Devil's Thumb Ranch, Colorado*.
2. Dobney, K., Baker, C. J., Quinn, A. D., & Chapman, L. (2009). Quantifying the effects of high summer temperatures due to climate change on buckling and rail related delays in south-east United Kingdom. *Meteorological Applications: A Journal of Forecasting, Practical Applications, Training Techniques and Modelling*, 16(2), 245–251. <https://doi.org/10.1002/met.114>
3. Dobney, K., Baker, C. J., Chapman, L., & Quinn, A. D. (2010). The future cost to the United Kingdom's railway network of heat-related delays and buckles caused by the predicted increase in high summer temperatures owing to climate change. *Proceedings of the Institution of Mechanical Engineers, Part F: Journal of Rail and Rapid Transit*, 224(1), 25–34. <https://doi.org/10.1243/09544097JRRT292>
4. Sanchis, I. V., Franco, R. I., Fernández, P. M., Zuriaga, P. S., & Torres, J. B. F. (2020). Risk of increasing temperature due to climate change on high-speed rail network in Spain. *Transportation Research Part D: Transport and Environment*, 82, 102312.
5. Thompson, W. C. (1991). Union pacific's approach to preserving lateral track stability. *Transportation Research Record*, 1289, 64–70.
6. Ling, L., Xiao, X. B., & Jin, X. S. (2014). Development of a simulation model for dynamic derailment analysis of high-speed trains. *Acta Mechanica Sinica*, 30(6), 860–875. <https://doi.org/10.1007/s10409-014-0111-0>
7. Martínez, I. N., Sanchis, I. V., Fernández, P. M., & Franco, R. I. (2015). Analytical model for predicting the buckling load of continuous welded rail tracks. *Proceedings of the Institution of Mechanical Engineers, Part F: Journal of Rail and Rapid Transit*, 229(5), 542–552. <https://doi.org/10.1177/0954409713518039>
8. Villalba Sanchis, I., Insa, R., Salvador, P., & Martínez, P. (2018). An analytical model for the prediction of thermal track buckling in dual gauge tracks. *Proceedings of the Institution of Mechanical Engineers, Part F: Journal of Rail and Rapid Transit*, 232(8), 2163–2172. <https://doi.org/10.1177/0954409718764194>
9. Ahmad, S. N., Mandal, N. K., & Chattopadhyay, G. (2009). A comparative study of track buckling parameters of continuous welded rail. In *Proceedings of the international conference on mechanical engineering* (pp. 26–28).
10. Ngamkhanong, C., Kaewunruen, S., & Costa, B. J. A. (2018). State-of-the-art review of railway track resilience monitoring. *Infrastructures*, 3(1), 3. <https://doi.org/10.3390/infrastructures3010003>
11. Chapman, L., Thornes, J. E., Huang, Y., Cai, X., Sanderson, V. L., & White, S. P. (2008). Modelling of rail surface temperatures: A preliminary study. *Theoretical and Applied Climatology*, 92(1), 121–131. <https://doi.org/10.1007/s00704-007-0313-5>
12. Oh, J. S., Khim, G., Oh, J. S., Park, C. H. (2012). Precision measurement of rail form error in a closed type hydrostatic guideway. *International Journal of Precision Engineering and Manufacturing*, 13(10), 1853–1859. <https://doi.org/10.1007/s12541-012-0243-8>
13. Wu, Y., Rasul, M. G., Powell, J., Micenko, P., & Khan, M. (2012). Rail temperature prediction model. In *Proceedings of the CORE 2012 global perspectives conference on railway engineering, Brisbane, Australia* (pp. 10–12).
14. Hong, S., Jung, H., Park, C., Lee, H., Kim, H., Lim, N., et al. (2019). Prediction of a representative point for rail temperature measurement by considering longitudinal deformation. *Proceedings of the Institution of Mechanical Engineers, Part F: Journal of Rail and Rapid Transit*, 233(10), 1003–1011. <https://doi.org/10.1177/0954409718822866>
15. Hong, S., Park, C., & Cho, S. (2021). A rail-temperature-prediction model based on machine learning: Warning of train-speed restrictions using weather forecasting. *Sensors*, 21(13), 4606. <https://doi.org/10.3390/s21134606>
16. Hong, S. U., Kim, H. U., Lim, N. H., Kim, K. H., Kim, H., & Cho, S. J. (2019). A rail-temperature-prediction model considering meteorological conditions and the position of the sun. *International Journal of Precision Engineering and Manufacturing*, 20(3), 337–346.
17. Urakawa, F., Watanabe, T., & Kimura, S. (2021). Wide-area rail temperature prediction method using GIS data. *Quarterly Report of RTRI*, 62(1), 61–66.
18. Whittingham HE and Commonwealth Bureau of Meteorology. Temperatures in exposed steel rails. Bureau of Meteorology.

Publisher's Note Springer Nature remains neutral with regard to jurisdictional claims in published maps and institutional affiliations.

Springer Nature or its licensor (e.g. a society or other partner) holds exclusive rights to this article under a publishing agreement with the author(s) or other rightsholder(s); author self-archiving of the accepted manuscript version of this article is solely governed by the terms of such publishing agreement and applicable law.



Cheoljeong Park received his B.S. degree at school of mechanical engineering of Chungnam National University, Korea, in 2018. Received his M.S. degree at department of mechanical engineering of Chungnam National University, Korea in 2020 and is currently in his Ph. D. degree at Chungnam National University, Korea since 2022. His research interests are in sensor fusion, computer vision, machine-learning and railway engineering.



Yeondo Jeong received his B.S. degree at school of mechanical engineering of Chungnam National University, Korea in 2019, received his M.S. degree at Chungnam National University, Korea in 2021 and is currently in HMC (Hyundai Motor Company) since 2021.



Jongwon Yoon received his B.S. degree at school of mechanical engineering of Chungnam National University, Korea, in 2020 and is currently in his M.S. degree at Chungnam National University, Korea since 2020. His research interests are in machine-learning prediction, deep-learning and sensors.



Jungmin Kim received his B.S. degree at school of mechanical engineering of Chungnam National University, Korea, in 2019 and is currently in his Ph. D. degree at Chungnam National University, Korea since 2019. His research interests are in MEMS, flexible sensors, biomimetics, photoelectrochemical cell and crack-based sensors.



Sunguk Hong received his B.S. and M.S degree at department of mechanical engineering of Chungnam national university, Korea, in 2017 and 2019, respectively. As researcher to ADD (Agency for Defense Development), Korea from 2019 to 2021, Sunguk Hong contributed to development, test and evaluation of unmanned ground vehicle system. Currently in his Ph. D. degree at POSTECH, Korea since 2022. His research interests are in human-robot interface, soft sensor, computer



Byeongjun Lee received his B.S. degree at school of mechanical engineering of Chungnam National University, Korea, in 2019, received his M.S degree in 2021 at Chungnam National University, Korea and is currently in his Ph.D. degree at Chungnam National University, Korea, since 2021. His research interests are in MEMS, NEMS, Electrospinning, Crack based strain sensor, Flexible strain sensor, Biomimetics.

vision, machine learning and mechanical simulations.



Chan Park received his B.S. degree at school of mechanical engineering of Chungnam National University, Korea, in 2017, received his M.S. degree at department of mechanical engineering of Chungnam National University, Korea in 2019 and is currently in his Ph.D. degree at Chungnam National University, Korea since 2019. His research interests are in MEMS/ NEMS, and flexible device.



Haran Lee received her B.S. degree at school of mechanical engineering of Hannam University, Korea, in 2019 and is currently in integrated Ph.D. program at Chungnam National University, Korea since 2020. Her research interests are in Membrane, Membrane Distillation, MEMS, Biomimetics, Bio-inspired sensors.



Chiwon Song received his B.S degree at school of mechanical engineering of Chungnam National University, Korea in 2022 and is currently in M.S. degree at Chungnam National University, Korea since 2022. His research interests are in MEMS, NEMS, Flexible strain sensor, strain sensor.



Seong J. Cho is associate professor at school of mechanical engineering of Chungnam national university, Korea. His research interests are in advanced sensor system, Nano/micro materials, MEMS/NEMS, advanced fabric, biomedical engineering, biomimetics, and bio-sensor.